THE JOURNAL OF PHYSICAL CHEMISTRY B
A JOURNAL OF THE AMERICAN CHEMICAL SOCIETY

Open Access
This article is licensed under CC-BY-NC-ND 4.0

pubs.acs.org/JPCB
Article

Acidic Conditions Impact Hydrophobe Transfer across the Oil–Water Interface in Unusual Ways

Published as part of The Journal of Physical Chemistry virtual special issue "Pablo G. Debenedetti Festschrift".

Sijia Chen, Zhefu Li, and Gregory A. Voth*

Cite This: *J. Phys. Chem. B* 2023, 127, 3911–3918
Read Online

ACCESS | Metrics & More | Article Recommendations | Supporting Information

ABSTRACT: Molecular dynamics simulation and enhanced free energy sampling are used to study hydrophobic solute transfer across the water–oil interface with explicit consideration of the effect of different electrolytes: hydronium cation (hydrated excess proton) and sodium cation, both with chloride counterions (i.e., dissociated acid and salt, HCl and NaCl). With the Multistate Empirical Valence Bond (MS-EVB) methodology, we find that, surprisingly, hydronium can to a certain degree stabilize the hydrophobic solute, neopentane, in the aqueous phase and including at the oil–water interface. At the same time, the sodium cation tends to "salt out" the hydrophobic solute in the expected fashion. When it comes to the solvation structure of the hydrophobic solute in the acidic conditions, hydronium shows an affinity to the hydrophobic solute, as suggested by the radial distribution functions (RDFs). Upon consideration of this interfacial effect, we find that the solvation structure of the hydrophobic solute varies at different distances from the oil–liquid interface due to a competition between the bulk oil phase and the hydrophobic solute phase. Together with an observed orientational preference of the hydroniums and the lifetime of water molecules in the first solvation shell of neopentane, we conclude that hydronium stabilizes to a certain degree the dispersal of neopentane in the aqueous phase and eliminates any salting out effect in the acid solution; i.e., the hydronium acts like a surfactant. The present molecular dynamics study provides new insight into the hydrophobic solute transfer across the water–oil interface process, including for acid and salt solutions.

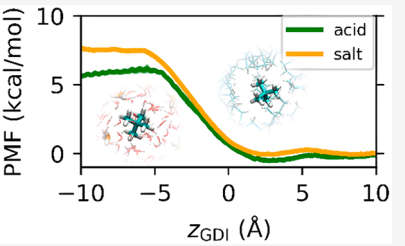

INTRODUCTION

Liquid–liquid interfaces widely exist in nature and play an essential role in many physical, chemical, and biological processes. For instance, solvent extraction of minerals,[1] transmembrane transport of drugs or nanoparticles,[2,3] and emulsification processes[4] are all related to immiscible liquids and their interfaces. However, liquid–liquid interfaces also remain less well understood due to the high mobility of the molecules and the thermal fluctuations of interfaces. It is noteworthy that only recently experimental techniques with time-resolved information have appeared. Surface-sensitive nonlinear spectroscopies, such as second harmonic generation[5,6] and vibrational sum-frequency spectroscopy,[7] can provide probe details of liquid–liquid interfaces. In addition to the structure of such interfaces, the transport of molecules and ions across liquid–liquid interfaces remains a complex and often unsolved problem. Electrochemical approaches have been extensively used to study the transport of organic and inorganic ions across different liquid–liquid interfaces.[8,9] However, there are still a relatively limited number experimental approaches to directly observe ion and molecular transport across liquid–liquid interfaces at the molecular scale.

On the other hand, molecular dynamics (MD) simulation provides the possibility to characterize such interfaces with atomic-scale resolution and by revealing thermodynamic and kinetic information. There has been notable effort devoted to studying the behavior of liquid–liquid interfaces with MD simulations.[10−13] Among them, the transfer of hydrophobic molecules across the interfaces is one of the most important phenomena and has been studied extensively (see, e.g., refs 14−16). However, most of these studies do not consider the influence of ions in the aqueous phase, especially hydrated excess protons (aka "hydronium").

Previous simulation work from this group first predicted that hydrated excess protons exhibit an unusual "amphiphilic" character leading these cations to have a distinct preference for the air–water interface.[17−20] In turn, this behavior results in the prediction of a marked interaction between hydronium and hydrophobic solutes in water for additional MD simulations.[21] This unusual and unique property of hydronium versus other simple cations suggests a different behavior may occur when hydrophobes transfer across acidic solution–oil interfaces as opposed to other salt solution–oil interfaces. This prediction is confirmed by this work.

Received: February 6, 2023
Revised: April 9, 2023
Published: April 21, 2023

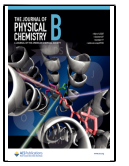

Downloaded via UNIV OF CHICAGO on September 16, 2024 at 18:17:37 (UTC).
See https://pubs.acs.org/sharingguidelines for options on how to legitimately share published articles.

ACS Publications
© 2023 The Authors. Published by American Chemical Society

https://doi.org/10.1021/acs.jpcb.3c00828
J. Phys. Chem. B 2023, 127, 3911−3918

In this work, we use the Multistate Empirical Valence Bond (MS-EVB) methodology to accurately simulate hydrated excess proton solvation and transport behavior, including its Grotthuss hopping transport.[22−25] Neopentane, which is arguably the smallest hydrocarbon molecule that can exhibit a strong hydrophobic effect, is used as the hydrophobic solute. While simple cations, like Na^+, salt out hydrophobic solutes from the aqueous phase,[26,27] we find that by contrast hydronium can stabilize the hydrophobic solutes in the aqueous phase and even more so at the oil−water interface. Through free energy calculations, we find that the acidic (dissociated HCl) conditions result in a considerably lower transfer free energy from the oil to the aqueous phase, compared to that in the dissociated NaCl salt conditions, by about 2−3 kcal/mol. The transfer free energy under the acidic conditions is even lower than that in the pure water case (no salt or acid). When examining the solvation structure of hydrophobic solutes in the acidic aqueous phase, a notable association of the hydrophobic solute molecules with hydrated excess protons in the is observed, which is quite different from that of the solutes with simple Na^+ cations.

METHODS

Simulation Details. The MS-EVB method was used to simulate hydrated protons with the MS-EVB 3.2 model.[25] The self-consistent iterative MS-EVB (SCI-MS-EVB) approach[28] enabled the treatment of multiple excess protons and hence more acidic conditions. SPC/Fw water model[29] and general Amber force field (GAFF)[30] was used to model water, and cyclohexane and neopentane, respectively. An Amber-compatible force field refined by Dang[31] was also used for Na^+ and Cl^-. For the system without any ions (denoted as the water system), the system was composed of 1 neopentane molecule, 400 water molecules, and 70 cyclohexane molecules. To construct a solution with acidic conditions, 15 excess protons, and 15 Cl^- anions were added to the water system (denoted as the acid system). For comparison purposes, the salt system was formed by replacing the excess protons of the acid system with Na^+ cations. Representative simulation snapshots of the acid and salt systems are shown in Figure 1. The simulation cells are periodic in all directions with dimensions of 21 × 21 × 60 $Å^3$. Initial configurations were established with PACKMOL[32] and the simulations were carried out with a modified SCI-MS-EVB version[33,34] of the LAMMPS MD software[35] with PLUMED.[36,37] All systems were first equilibrated for 2 ns using classical MD simulation (namely, without the MS-EVB method for the acid system) in the constant *NPT* ensemble with the Nosé−Hoover thermostat and barostat with a target temperature of 298 K and a target pressure of 1 atm. The relaxation constants for the thermostat and the barostat were 100 and 1000 fs, respectively. The x and y dimensions were coupled during the equilibration to ensure a square interface. The cutoff for the Lennard-Jones and short-range Coulombic interaction was 9 Å. The long-range electrostatic interactions were calculated by Ewald summation with a relative precision of 10^{-5}. Next, the MS-EVB method was employed for the acid system in the constant *NPT* ensemble for another 400 ps of equilibration. The last snapshot of the equilibration run was used for the subsequent production run. All production runs were conducted in the constant *NVT* ensemble with a Nosé−Hoover thermostat having a relaxation constant of 100 fs to maintain the temperature at 298 K. Umbrella sampling was employed in the production run. For each umbrella sampling window, 2 ns trajectories for the acid system and 8 ns trajectories for the salt and water systems of production data were collected. Details about the umbrella sampling can be found in the Results and Discussion.

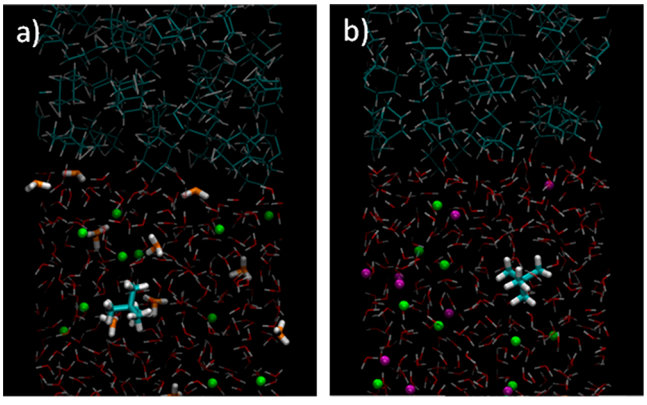

Figure 1. Representative MD simulation snapshots of the (a) acid and (b) salt systems when the neopentane molecule is in the bulk aqueous phase. The neopentane molecule and hydrated excess protons are represented, respectively, as licorice (with the carbon atoms colored cyan) and the hydronium cation oxygen atoms are colored orange. Na^+ and Cl^- ions are depicted as purple and green spheres, respectively.

RESULTS AND DISCUSSION

Free Energy Profile of Hydrophobe Transfer Across the Water−Oil Interface. Umbrella sampling was employed to calculate the free energy of hydrophobe transfer across the water−oil interface. The z component of the center of mass (COM) of the neopentane molecule was restrained with a harmonic bias $U(z) = K_z(z - z_0)^2/2$, with K_z = 20 kcal mol^{-1} $Å^2$, using z_0 between −12 Å and +10 Å in 45 evenly spaced umbrella windows. To correctly account for the transfer free energy differences in the three systems, we also employed an alternative coordinate z_{GDI}, the distance from the object (position of an atom, center of mass of a molecule, etc.) to the Gibbs dividing interface (GDI) of water; a negative value indicates that the object is in the aqueous phase, while a positive value indicates that it is in the oil phase. The z_{GDI} provides a way to systematically describe an object's position relative to the water−oil interfaces in different systems. The GDI is a plane normal to the z-axis where the local density of water is half of that in bulk on average. The GDIs of acid, salt, and water systems are located at z = −1.3, −1.0, and −2.0 Å, respectively.

The potential of mean force (PMF) for the center of mass (COM) of the neopentane molecule's z_{GDI} was calculated by the weighted histogram analysis method (WHAM),[38] with the results shown in Figure 2. Clearly, while in any of the systems the neopentane has a strong thermodynamic driving force to leave the aqueous phase and go into the oil phase, the neopentane in the acid system has lower free energy in the aqueous phase than in the aqueous salt and even (to a small degree) in the pure water systems. Neopentane is more stable in the acid system than in the salt system by about 2.2 kcal/mol. It is even more stable in acid than in the water system by about 0.4 kcal/mol in the bulk aqueous phase. The considerable decrease in the free energy suggests that the coexistence of hydronium cations with the neopentane in the aqueous phase helps to stabilizes the neopentane molecule to a clear degree, while in the salt solution the neopentane is more destabilized (salted out). This result also

https://doi.org/10.1021/acs.jpcb.3c00828
J. Phys. Chem. B 2023, 127, 3911−3918

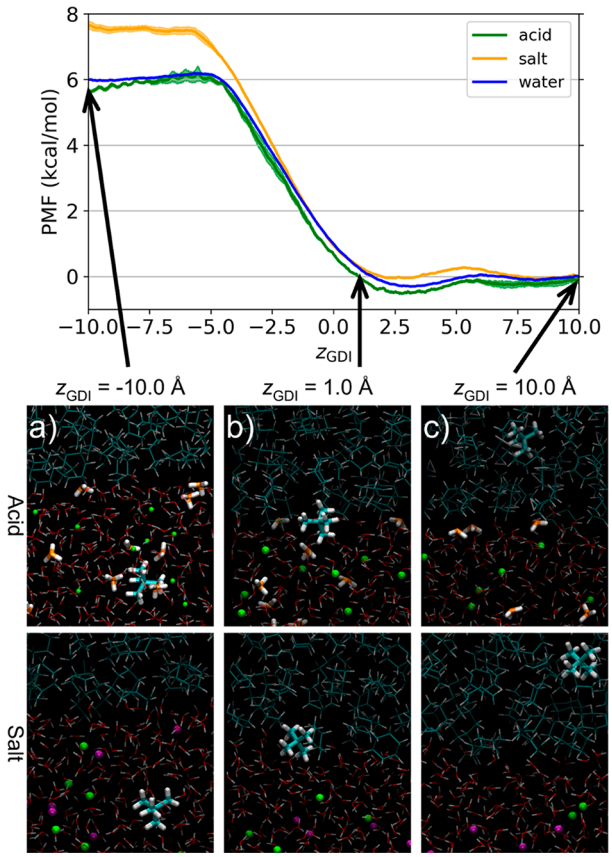

Figure 2. Potential of mean force (PMF) as a function of the distance from the Gibbs dividing interface (GDI) of water, z_{GDI}, for acid solution (green curve), salt solution (orange curve), and water (blue curve) systems. The shadings denote the standard error. Negative values of z_{GDI} correspond to the aqueous phase, while positive values correspond to the oil (cyclohexane) phase. Panels (a–c): Representative molecular dynamics simulation snapshots of the acid and salt systems when the neopentane molecule is in aqueous phases, interfacial regions, and oil phases as denoted by the black arrows in the upper figure. The neopentane molecules are represented as licorice along with the hydrated proton structures, for which the carbon atoms are colored cyan and the oxygen atoms are colored orange, while Na^+ and Cl^- are depicted as purple and green spheres.

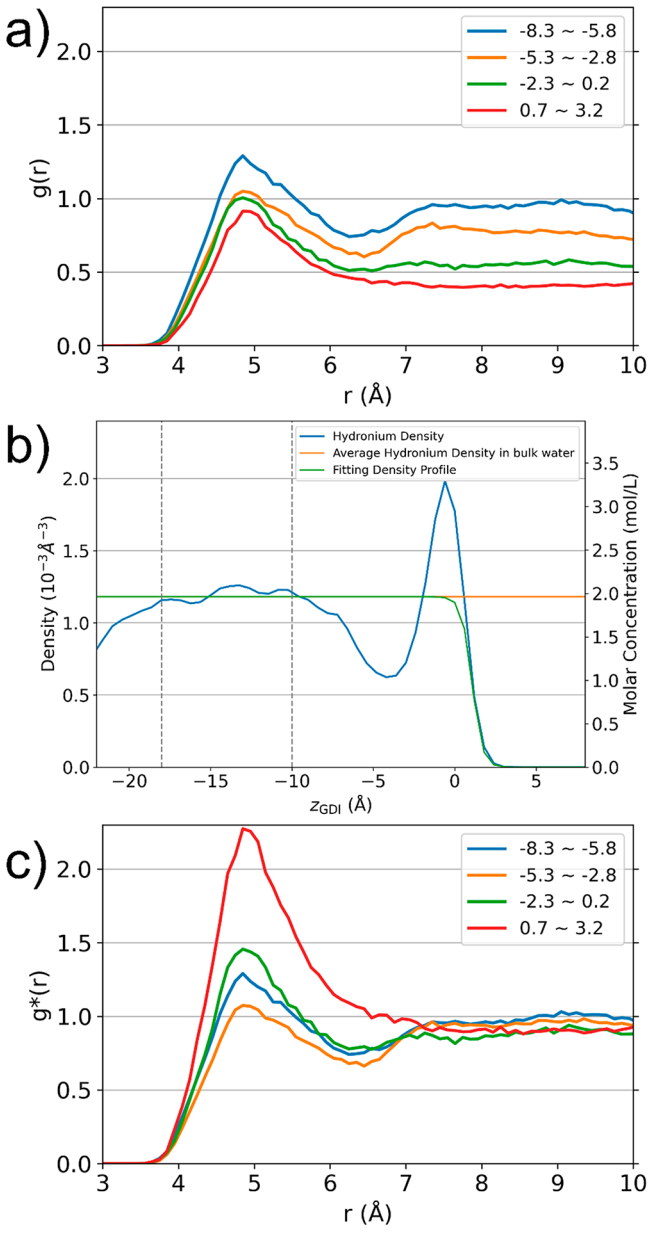

Figure 3. (a) Original and (c) modified RDFs between the central carbon (CC) of the neopentane molecule and most probable hydronium oxygens (O_H) in the acid system when the neopentane molecule is biased in different regions. The legends show the position where the neopentane molecule is biased relative to the GDI of water. (b) The density profile of the hydronium (blue line) in the acid system and the fitting curve (green line) using eq 1. The data between the two vertical dashed lines are used for the calculation of average hydronium density in the central aqueous phase.

coincides with experiments,[39−43] which find that highly acidic conditions can enhance the solubility of hydrophobic solutes compared to the salt condition.

Solvation Structure of Neopentane in Different Systems. The free energy differences due to the coexistence of different cations suggest distinct solvation structures near the hydrophobic molecule, which can be quantified in terms of the radial distribution function (RDF), $g(r)$. In order to illustrate the marked association between hydroniums and hydrophobic solutes, RDFs between the central carbon (CC) atom of the neopentane molecule and most probable hydronium-like oxygens (O_H) when the neopentane molecule is in different z_{GDI} regions are shown in Figure 3(a). Due to the fact that this is an interface system, we take the average density of the hydronium in the central aqueous phase (see Figure 3(b)) as the reference average density that divides the number of counted particles when calculating the RDFs. As manifested by the primary peaks in the RDFs at $r \approx 4.9$ Å and by the absence of a secondary peak, we can conclude that there is a significant affinity between the hydroniums and the neopentane molecule. By integrating the four RDFs to the first minimum $r \approx 6.25$ Å, we can get the coordination numbers of the hydrated proton with the neopentane in different region, which are 0.84, 0.70, 0.62, and 0.55, respectively, as the neopentane becomes closer to the interface. As the neopentane nears the interface, there is less aqueous phase around the neopentane, therefore the coordination number decreases. By contrast, as shown in the RDFs between CC atoms and Na^+ cations in the salt systems (Figure 4(a)), there is a much lower primary peak in the RDFs between CC atom and Na^+ appear at $r \approx 7.1$ Å when the neopentane molecule is not so close to the GDI. At the same time, there is no

https://doi.org/10.1021/acs.jpcb.3c00828
J. Phys. Chem. B 2023, 127, 3911−3918

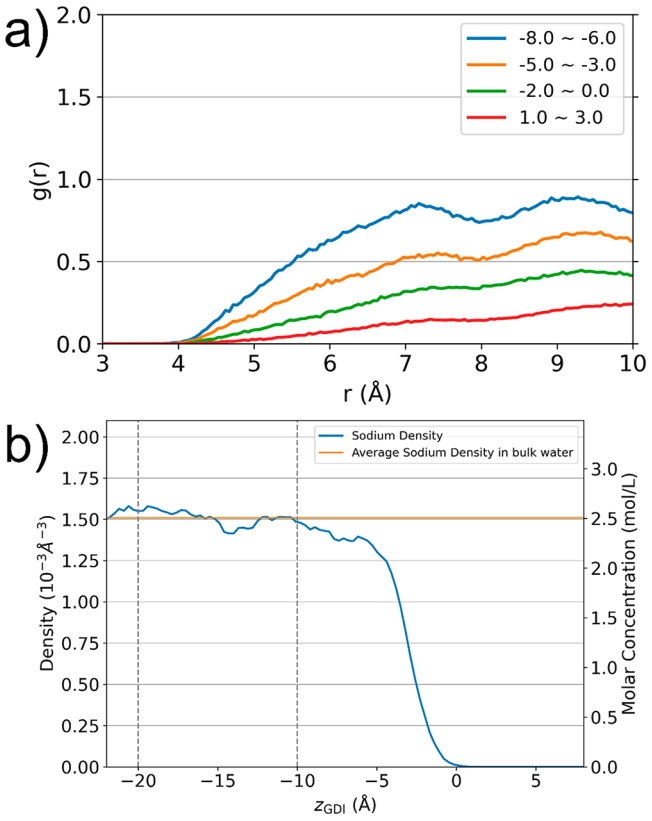

Figure 4. (a) Original RDFs between the central carbon (CC) of the neopentane molecule and Na^+ cations in the salt system when the neopentane molecule is biased in different regions. The legends show the position where the neopentane molecule is biased relative to the GDI of water. (b) The density profile of Na^+ cations (blue line) in the salt system and the average Na^+ density (orange line) in the bulk water region.

obvious peak in the RDFs when the neopentane molecule gets closer to the GDI since the local density of nearby Na^+ keeps decreasing (as shown in Figure 4(b)). However, in the acid systems, when the neopentane molecule gets closer to the GDI, there is no noticeable decrease in the heights of the primary peaks in the three regions (z_{GDI} = −5.3 to −2.8 Å, z_{GDI} = −2.3 to −0.2 Å, z_{GDI} = 0.7 to 3.2 Å) compared to the salt system. Further explanation is necessary to understand this unusual phenomenon, which can be attributed to the hydrated proton's affinity for the hydrophobic/hydrophilic interface. This affinity results in a larger density of hydrated protons at the water−oil interface, leading to a higher occurrence of hydrated protons around the neopentane molecule. In fact, it has been extensively discussed and confirmed by experiments and simulations[17,19,44,45] that the hydrated excess proton shows an affinity for the simplest hydrophobic/hydrophilic interface, the air−water interface, under acidic solution conditions, thus contradicting more conventional concepts that cations are buried into the bulk. Such behavior is also observed in the case of the hydrophobic solutes in the acid aqueous phase, where the hydrated protons exhibit an amphiphilic property and therefore an association propensity with the hydrophobic solutes in acid solution.[21] It is not surprising that the hydrated proton shows this unique behavior again at the water−oil interface, as indicated by the density profile of hydronium (as shown in Figure 3(b)).

When looking at the density profile of hydronium (as shown in Figure 3(b)), from the bulk aqueous phase to the water−oil interface, the density of hydronium first decreases, then suddenly goes up and reaches its maximum density at $z_{GDI} \approx$ −0.5 Å, and finally drops to zero. Such vanishing hydronium density affects the RDFs in an undesirable way. Although there is no ion at all in the oil phase, we still take the volume of that part into account when calculating the RDFs. The first drawback is that the RDFs will never converge to 1, which is what RDFs should do. The second side effect is the influence of the vanishing density mixes with the enhanced density at the interface. For clearer insight, it is always necessary to eliminate the effect of the vanishing density, since we are not concerned with the zero-density zone. To eliminate the effect of vanishing hydronium density above the GDI and better illustrate the association between hydronium and neopentane at different values of z_{GDI}, we introduced a modified RDF, $g^*(r)$. First, the density profile of hydronium in each window was obtained. Part of the data, which are less than 90% of bulk density and keep dropping to zero, are used to fit terms of a Fermi function

$$\rho_i(z) = \rho_0 \cdot \frac{1}{1 + \exp(-a_i z + b_i)} \tag{1}$$

where a_i and b_i are fitting parameters for the ith window and ρ_0 is the density of hydronium in bulk water (average density between z_{GDI} = −18 Å and z_{GDI} = −10 Å). Then, RDFs are calculated for each window, $g(r,z_i)$, where z_i is the average position of the COM of neopentane in the ith window. A modification factor $f(r,z_i)$ is defined as

$$f(r, z_i) = \frac{1}{2r} \int_{z_i - r}^{z_i + r} \frac{1}{1 + \exp(-a_i z + b_i)} \, dz \tag{2}$$

Next, the final modified RDF can be given by

$$g^*(r, z_i) = g(r, z_i)/f(r, z_i) \tag{3}$$

This modification removes the effect of the final drop in concentration but retains the impact of the other information, like hydronium's adsorption behavior to the water−oil interface. The modified RDFs are again averaged in the four regions, as shown in Figure 3(c). First, it is convincing to see that the modified RDFs are nearly converging to 1, which indicates that our modification is appropriate. Although there are small differences, we may attribute these to statistical error, since the simulation time is limited, and the density profile of hydronium fluctuates. The major differences between $g(r)$ and $g^*(r)$ are the heights of primary peaks for different regions. When the neopentane molecule is close to the bulk water (z_{GDI} = −8.3 to −5.8 Å), the height of the primary peak of $g^*(r)$ is about 1.3, which is identical to the original RDF since the interface does not affect the primary peak of the RDF when the neopentane is far away from the interface. When the neopentane molecule is above the GDI (z_{GDI} = 0.7−3.2 Å), the primary peak of $g^*(r)$ is the highest among the four peaks, suggesting the strongest association. This association between hydroniums and the neopentane molecule above the GDI is a direct result of the unusual amphiphilic property of hydronium. Due to the existence of the water−cyclohexane hydrophilic−hydrophobic interface, hydroniums exhibit a strong affinity to this interface and therefore have a higher local density in the region of $z_{GDI} \approx$ −1.5 to +0.5 Å (see the density profile of hydronium in Figure 3(b)). This higher local density of hydronium results in the higher height of the primary peak of $g^*(r)$ since hydroniums in this region contribute most to the primary peak. However, when the neopentane molecule is neither deep in the bulk water nor

https://doi.org/10.1021/acs.jpcb.3c00828
J. Phys. Chem. B 2023, 127, 3911−3918

close enough to the interface (z_{GDI} = −5.3 to −2.8 Å), the primary peak of $g^*(r)$ in this region is the lowest. This phenomenon results from the competition between the water−cyclohexane interface and the water−neopentane interface for hydroniums. Obviously, the water−cyclohexane interface is considerably larger than the water−neopentane one and therefore is more attractive to hydroniums. This leads to a much lower primary peak for $g^*(r)$ in this region, and the local density of hydronium in this region is also the lowest compared to other regions. When it comes to the region in the middle of the two regions mentioned above (z_{GDI} = −2.3 to 0.2 Å), the height of the primary peak after modification is also between two extremes since one side is next to the low-density region and the other side is in contact with the high-density region. We can thus conclude that the modified RDFs not only confirm the marked association between the hydrophobic solute and hydroniums but also reflect the solvation structure differences when the neopentane molecule is at different values of z_{GDI}.

Except for the RDF itself, we can also probe the interaction strength between the hydronium and the neopentane by calculating the potential of mean force (PMF) from inversion of the RDF via the reversible work theorem. Details of this calculation can be found from the Supporting Information. Generally speaking, there is always attraction between the hydronium and the neopentane, suggested by a well in the PMF near r = 4.85 Å, as shown in Figure S2. When the neopentane is quite close to the interface, the depth of the well is about 0.486 kcal/mol, while when the neopentane is neither deep in the bulk water nor close enough to the interface, the well depth is only about 0.042 kcal/mol. The above observation suggests that the association between the hydronium and the neopentane is largely dependent on the position of the neopentane relative to the interface, consistent with our above analysis.

Orientational Preference of the Hydrated Excess Protons with Respect to Neopentane. According to earlier transfer free energy and solvation structure analysis, it became clear that the existence of hydrated excess protons can enhance the solubility of the hydrophobic species, neopentane, in the aqueous phase and also near the oil−water interface. It is therefore important to examine the molecular structure of the hydrated excess proton surrounding the hydrophobic neopentane in more detail to better resolve the unique "amphiphilic" characteristic of the hydrated protons. Previous simulation studies[17−20] concluded that the disruption of the hydrogen-bond network caused by the hydrated excess proton results in a propensity for the Eigen cation to the water−air interface, with the lone electron pair of hydronium oxygen pointing away from the interface into the air. A similar phenomenon is observed in this system based on the orientational preference of the hydrated excess protons surrounding the neopentane. In order to characterize the orientational preference, we define the angle θ between the vector connecting the OH to the CC of neopentane, denoted by $\vec{R}_{OH-CC}$, and the vector connecting the O_Hs to the corresponding geometric center of three hydrogen atoms of the hydronium (HC), denoted by $\vec{R}_{OH-HC}$. As shown in Figure 5, the dependence of the probability distribution profiles of θ, $P(\theta)$, on the distance between CC and OH, r_{CC-OH}, illustrates the apparent orientational preference of the hydronium to have its lone pair side toward the hydrophobic neopentane when $\vec{R}_{OH-CC}$ < 4.5 Å, as indicated by the pronounced peak around 140°. When it comes to the 4.5 Å < $\vec{R}_{OH-CC}$ < 5.5 Å region, the preference still exists, but it is less pronounced. When

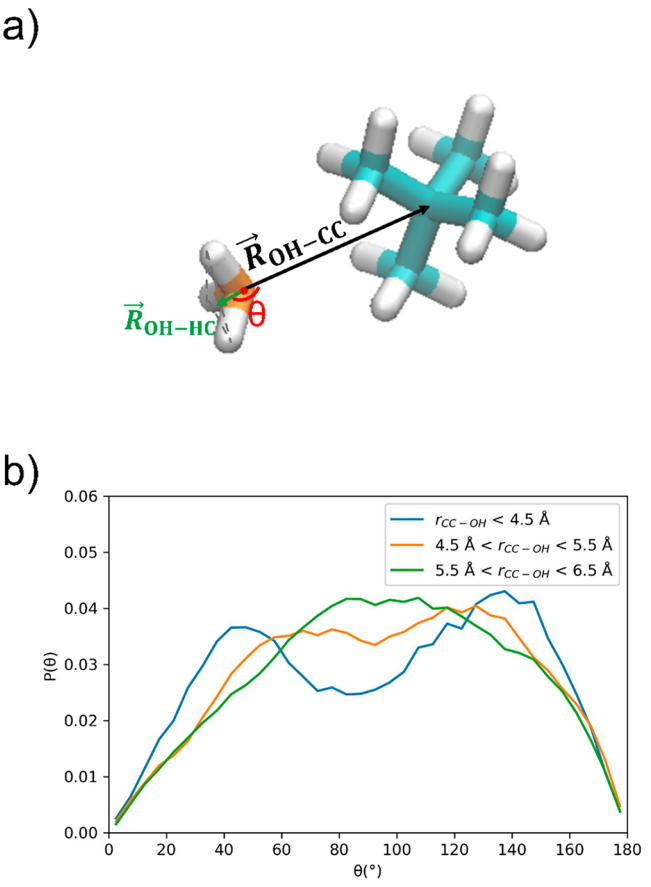

Figure 5. (a) Illustration of the definition of the relative orientation of the hydrated excess proton with respect to neopentane. (b) Probability distribution profiles of the relative orientation between hydrated excess protons and neopentane, as a function of the distance between the central carbon (CC) atom of the neopentane molecule and the most probable hydronium oxygens (O_H) in the acid system.

hydronium becomes farther away from the neopentane molecule, like 5.5 Å < $\vec{R}_{OH-CC}$ < 6.5 Å, the hydrated excess proton loses its orientational preference toward neopentane.

The additional peaks around 40° (when $\vec{R}_{OH-CC}$ < 4.5 Å) and 60° (when 4.5 Å < $\vec{R}_{OH-CC}$ < 5.5 Å) can be attributed to the existence of the Cl^- counterion.[21] The electrostatic attraction between Cl^- and the three hydronium hydrogen atoms enforces the positively charged hydrogens facing toward Cl^-. Overall, despite of the involvement of the Cl^- counterion, the hydrated excess proton tends to orient its hydrophobic lone electron pair side toward the hydrophobic neopentane molecule. This reorientation behavior facilitates reducing the hydrophobic/hydrophilic interaction between neopentane and the aqueous phase, which in turn stabilizes the existence of neopentane in the aqueous phase.

Average Lifetime of Water Molecules in the First Solvation Shell of Neopentane. Except for the ions, water molecules in the first few solvation shells of neopentane also play an important role in the solvation behavior. Water molecule exchange dynamics is one of the most important characteristics of water solvation shells, which can be quantified by the lifetime of water molecules in the first solvation shell. Accordingly, we used a time correlation function to evaluate the lifetime of water molecules in the first hydration shell of neopentane, defined as

https://doi.org/10.1021/acs.jpcb.3c00828
J. Phys. Chem. B 2023, 127, 3911−3918

$$C_{WL}(t) = \frac{\langle h(0)\cdot h(t)\rangle}{\langle h\rangle} \quad (4)$$

in which $h(t) = 1$ if a certain water molecule is in the first solvation shell of neopentane and $h(t) = 0$ if it is not. The $\langle\cdots\rangle$ symbol denotes the ensemble average over the entire MD simulation trajectory and all water molecules. This autocorrelation function describes the possibility of a certain water molecule remaining in the first solvation shell after a certain amount of time t. The correlation function can be well fit by an exponential decay:

$$C_{WL}(t) = \exp\left(-\frac{t}{\tau_1}\right) \quad (5)$$

Therefore, the lifetime of water molecules for a given system can be obtained by τ_1.

The average lifetimes of water molecules in the first solvation shell of neopentane as a function of z_{GDI} for acid, salt, and water systems are shown in Figure 6. Clearly, the lifetime of water in the first solvation shell of neopentane in the acid system is significantly longer than that in the water or salt system, more than twice the latter two. This can be ascribed to the existence of hydronium in the first solvation shell. As we mentioned above, the Eigen cation prefers hydrophobic−hydrophilic interfaces, due to the interruption of the hydrogen network caused by the hydrated excess proton. In the current system, this amphiphilic characteristic can stabilize the hydrogen-bond network near the neopentane/water interface, resulting in the increase in lifetime. The slightly higher lifetime of the salt system than water systems can be explained by Cl^- anions in the first few solvation shells, which slightly decrease the number of water molecules and reduces the possibility of exchange of water molecules. Examining the lifetime of water molecules thus provides new insight into how ions can affect the solvation of hydrophobes in the aqueous phase and further demonstrates that hydrated excess protons contribute to an enhanced solubility of hydrophobes in acidic aqueous solutions.

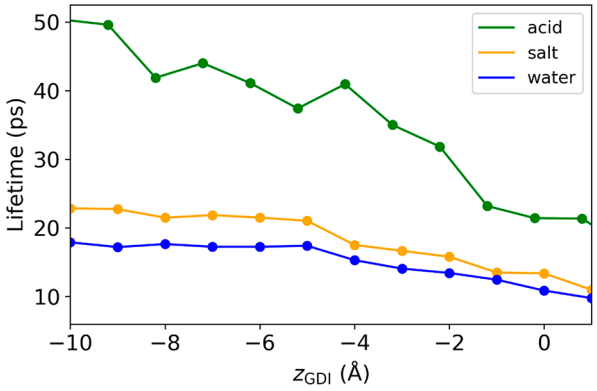

Figure 6. Average lifetime of water molecules in the first solvation shell of neopentane as a function of the distance from the Gibbs dividing interface (GDI) of water, z_{GDI}, for acid (green line), salt (orange line), and water (blue line) systems.

Anomaly of the Solvation of Hydrophobe in Acid Solution Than Other Electrolytes. In the previous sections, we demonstrated that neopentane exhibits different behavior in acidic HCl solution than in NaCl solution, which can influence its transfer from the aqueous phase to the oil phase as indicated by the PMF. The solvation of hydrophobic species in the aqueous solution and its transfer between hydrophilic−hydrophobic interfaces plays a crucial role in diverse disciplines, including interfacial science, emulsification process, biomolecular assemblies, etc.[46−50] The central challenge in understanding the aggregation/dissociation of hydrophobic particles in water lies in capturing how the enthalpy and entropy of neighboring water molecules and the solute itself interplay with each other. The hydrophobic solutes will not only interact between themselves and with the water molecules, but also cause hydrogen bonding rearrangements in its vicinity. It is not surprising that such an effect is sensitive to the properties of the solutes itself,[46,51,52] including its size, shape, curvature, and the chemical nature, and the conditions of the solution, such as temperature,[52,53] ionic strength,[54] and existence of cosolutes.[55]

One important application related to an understanding of hydrophobicity is to address problems of salt effects on molecular (e.g., proteins) stability and denaturation or enzymatic activity. The famous Hofmeister series qualitatively arranges the cations and anions by their ability to "salt-out" proteins.[26,27,56] Generally speaking, larger cations always prefer to salt out proteins compared to smaller cations.[57] However, although a hydrated proton shares a similar size with the salting-out cation K^+, the online NIST solubility databases reveal that the salting-out effect of small hydrocarbons in HCl solutions is significantly weaker than that for other salt solutions. For example, the ambient gas solubility of butane can be reduced by 40% in 1 mol/kg NaCl solution compared to in pure water, while only a 10% reduction was found in 1 mol/kg HCl solution.[43,58] The mechanism behind this behavior cannot be simply attributed to the hydration energy of cations, which is inversely dependent on the ionic radius, but also to the amphiphilic character and unique physics of the hydrated proton, as we have pointed out previously.[21] In addition, the primary peaks of the RDFs between the CC and Cl^- in the acid system, as shown in the Figure S3(a), indicate an enhanced number of anions around the hydrophobe. This cannot be simply ascribed to anion absorption at the hydrophobe/water interface[59] due to the dangling hydrogen bonds of the interfacial water molecules,[60] since the peaks in the acid condition are higher than those in the salt conditions (see Figure S3(b)). Because of the association between the neopentane and the hydrated proton, they form a positively charged "hydrophobe-hydrated proton core", making the contact ion pair peak of Cl^- with the hydrated proton become dominant in the RDFs. Moreover, the unique physics and chemistry of the hydrated proton make it an anomaly in the Hofmeister series, and this is essential to consider this when addressing related issues.

CONCLUDING REMARKS

The present work explores hydrophobe transfer across the water−oil interface with explicit consideration of aqueous ions, including acidic conditions. It provides new information on the enhanced stability of hydrophobic solutes in acidic solutions compared to salt solutions. Using neopentane as an example of a hydrophobic solute, the results illustrate the interplay of the hydrated excess proton's amphiphilic character with the hydrophobic solute both in the aqueous phase and at the water−oil interface. Compared to the simple ion Na^+, the existence of a hydrated proton considerably decreases the free energy of the hydrophobic solute transfer from the oil to the aqueous phase by about 2−3 kcal/mol. The results further demonstrate the pronounced association between neopentane and hydronium cations through a solvation structure analysis of

https://doi.org/10.1021/acs.jpcb.3c00828
J. Phys. Chem. B 2023, 127, 3911−3918

the hydrophobic solute. This kind of association changes at different values of z_{GDI} due to the competition between the two hydrophobic−hydrophilic interfaces: neopentane−water and cyclohexane−water.

The observations in this work are consistent with our previous studies on hydronium at the air−water interface and neopentane in bulk acid solution.[17,19−21] The study of how acidic conditions affect the partitioning of hydrophobic solutes in water−oil systems can shed new light on the underlying forces involved in separation science, drug distribution in pharmacokinetics, and nanoparticle synthesis. Additionally, analyzing the dynamics of hydronium around hydrophobic species, such as its lifetime, orientation correlation function, and hydrogen-bond networks, can provide further insight into these behaviors. To gain a deeper understanding of the related mechanisms and to uncover new insights into these topics, we will conduct future studies that investigate hydrophobes of varying sizes and more polar solutes, accompanied by in-depth analysis of both thermodynamics and dynamics.

■ ASSOCIATED CONTENT

Supporting Information

The Supporting Information is available free of charge at https://pubs.acs.org/doi/10.1021/acs.jpcb.3c00828.

Density profiles of the anion, PMF of the association between neopentane and hydronium, RDFs between neopentane and the anion (PDF)

■ AUTHOR INFORMATION

Corresponding Author

Gregory A. Voth − *Department of Chemistry, Chicago Center for Theoretical Chemistry, The James Franck Institute, and Institute for Biophysical Dynamics, The University of Chicago, Chicago, Illinois 60637, United States;* orcid.org/0000-0002-3267-6748; Email: gavoth@uchicago.edu

Authors

Sijia Chen − *Department of Chemistry, Chicago Center for Theoretical Chemistry, The James Franck Institute, and Institute for Biophysical Dynamics, The University of Chicago, Chicago, Illinois 60637, United States;* orcid.org/0000-0003-2060-4920

Zhefu Li − *Department of Chemistry, Chicago Center for Theoretical Chemistry, The James Franck Institute, and Institute for Biophysical Dynamics, The University of Chicago, Chicago, Illinois 60637, United States*

Complete contact information is available at: https://pubs.acs.org/10.1021/acs.jpcb.3c00828

Notes

The authors declare no competing financial interest.

■ ACKNOWLEDGMENTS

This research was supported by the U.S. Department of Energy, Office of Basic Energy Sciences, Separation Science Program of the Division of Chemical Sciences, Geosciences, and Biosciences, under Award Number DE-SC0018648. The computational resources for this research were provided by the University of Chicago Research Computing Center (RCC).

■ REFERENCES

(1) Riano, S.; Binnemans, K. Extraction and Separation of Neodymium and Dysprosium from Used NdFeB Magnets: An Application of Ionic Liquids in Solvent Extraction Towards the Recycling of Magnets. *Green Chem.* **2015**, *17*, 2931−2942.

(2) Benson, S. P.; Pleiss, J. Molecular Dynamics Simulations of Self-Emulsifying Drug-Delivery Systems (SEDDS): Influence of Excipients on Droplet Nanostructure and Drug Localization. *Langmuir* **2014**, *30*, 8471−8480.

(3) Nademi, Y.; Tang, T.; Uludag, H. Steered Molecular Dynamics Simulations Reveal a Self-Protecting Configuration of Nanoparticles During Membrane Penetration. *Nanoscale* **2018**, *10*, 17671−17682.

(4) Bouchemal, K.; Briancon, S.; Perrier, E.; Fessi, H. Nano-Emulsion Formulation Using Spontaneous Emulsification: Solvent, Oil and Surfactant Optimisation. *Int. J. Pharm.* **2004**, *280*, 241−251.

(5) Shen, Y. R. Optical Second Harmonic Generation at Interfaces. *Annu. Rev. Phys. Chem.* **1989**, *40*, 327−350.

(6) Petersen, P. B.; Saykally, R. J. Probing the Interfacial Structure of Aqueous Electrolytes with Femtosecond Second Harmonic Generation Spectroscopy. *J. Phys. Chem. B* **2006**, *110*, 14060−14073.

(7) Nihonyanagi, S.; Mondal, J. A.; Yamaguchi, S.; Tahara, T. Structure and Dynamics of Interfacial Water Studied by Heterodyne-Detected Vibrational Sum-Frequency Generation. *Annu. Rev. Phys. Chem.* **2013**, *64*, 579−603.

(8) Herzog, G. Recent Developments in Electrochemistry at the Interface between Two Immiscible Electrolyte Solutions for Ion Sensing. *Analyst* **2015**, *140*, 3888−3896.

(9) Lima, H. R. S.; da Silva, J. S.; de Oliveira Farias, E. A.; Teixeira, P. R. S.; Eiras, C.; Nunes, L. C. C. Electrochemical Sensors and Biosensors for the Analysis of Antineoplastic Drugs. *Biosens. Bioelectron.* **2018**, *108*, 27−37.

(10) Benjamin, I. Molecular Structure and Dynamics at Liquid-Liquid Interfaces. *Annu. Rev. Phys. Chem.* **1997**, *48*, 407−451.

(11) Walker, D. S.; Moore, F. G.; Richmond, G. L. Vibrational Sum Frequency Spectroscopy and Molecular Dynamics Simulation of the Carbon Tetrachloride-Water and 1,2-Dichloroethane-Water Interfaces. *J. Phys. Chem. C* **2007**, *111*, 6103−6112.

(12) Benjamin, I. Reaction Dynamics at Liquid Interfaces. *Annu. Rev. Phys. Chem.* **2015**, *66*, 165−188.

(13) Morita, A.; Koizumi, A.; Hirano, T. Recent Progress in Simulating Microscopic Ion Transport Mechanisms at Liquid-Liquid Interfaces. *J. Chem. Phys.* **2021**, *154*, 080901.

(14) Pohorille, A.; Wilson, M. A. Excess Chemical Potential of Small Solutes across Water-Membrane and Water-Hexane Interfaces. *J. Chem. Phys.* **1996**, *104*, 3760−3773.

(15) Bemporad, D.; Essex, J. W.; Luttmann, C. Permeation of Small Molecules through a Lipid Bilayer: A Computer Simulation Study. *J. Phys. Chem. B* **2004**, *108*, 4875−4884.

(16) Zahariev, T. K.; Tadjer, A. V.; Ivanova, A. N. Transfer of Non-Ionic Surfactants across the Water-Oil Interface: A Molecular Dynamics Study. *Colloids Surf., A* **2016**, *506*, 20−31.

(17) Petersen, M. K.; Iyengar, S. S.; Day, T. J. F.; Voth, G. A. The Hydrated Proton at the Water Liquid/Vapor Interface. *J. Phys. Chem. B* **2004**, *108*, 14804−14806.

(18) Iuchi, S.; Chen, H.; Paesani, F.; Voth, G. A. Hydrated Excess Proton at Water-Hydrophobic Interfaces. *J. Phys. Chem. B* **2009**, *113*, 4017−4030.

(19) Li, Z.; Li, C.; Wang, Z.; Voth, G. A. What Coordinate Best Describes the Affinity of the Hydrated Excess Proton for the Air-Water Interface? *J. Phys. Chem. B* **2020**, *124*, 5039−5046.

(20) Tse, Y.-L. S.; Chen, C.; Lindberg, G. E.; Kumar, R.; Voth, G. A. Propensity of Hydrated Excess Protons and Hydroxide Anions for the Air-Water Interface. *J. Am. Chem. Soc.* **2015**, *137*, 12610−12616.

(21) Chen, H.; Xu, J.; Voth, G. A. Unusual Hydrophobic Interactions in Acidic Aqueous Solutions. *J. Phys. Chem. B* **2009**, *113*, 7291−7.

(22) Schmitt, U. W.; Voth, G. A. The Computer Simulation of Proton Transport in Water. *J. Chem. Phys.* **1999**, *111*, 9361−9381.

(23) Day, T. J. F.; Soudackov, A. V.; Ćuma, M.; Schmitt, U. W.; Voth, G. A. A Second Generation Multistate Empirical Valence Bond Model

for Proton Transport in Aqueous Systems. *J. Chem. Phys.* **2002**, *117*, 5839−5849.
(24) Wu, Y.; Chen, H.; Wang, F.; Paesani, F.; Voth, G. A. An Improved Multistate Empirical Valence Bond Model for Aqueous Proton Solvation and Transport. *J. Phys. Chem. B* **2008**, *112*, 467−82.
(25) Biswas, R.; Tse, Y. L.; Tokmakoff, A.; Voth, G. A. Role of Presolvation and Anharmonicity in Aqueous Phase Hydrated Proton Solvation and Transport. *J. Phys. Chem. B* **2016**, *120*, 1793−804.
(26) Hofmeister, F. Zur Lehre Von Der Wirkung Der Salze. *Arch. Exp. Pathol. Pharmakol.* **1888**, *24*, 247−260.
(27) Baldwin, R. L. How Hofmeister Ion Interactions Affect Protein Stability. *Biophys. J.* **1996**, *71*, 2056−2063.
(28) Wang, F.; Voth, G. A. A Linear-Scaling Self-Consistent Generalization of the Multistate Empirical Valence Bond Method for Multiple Excess Protons in Aqueous Systems. *J. Chem. Phys.* **2005**, *122*, 144105.
(29) Wu, Y.; Tepper, H. L.; Voth, G. A. Flexible Simple Point-Charge Water Model with Improved Liquid-State Properties. *J. Chem. Phys.* **2006**, *124*, 024503.
(30) Wang, J.; Wang, W.; Kollman, P. A.; Case, D. A. Automatic Atom Type and Bond Type Perception in Molecular Mechanical Calculations. *J. Mol. Graphics Modell.* **2006**, *25*, 247−60.
(31) Dang, L. X. Mechanism and Thermodynamics of Ion Selectivity in Aqueous Solutions of 18-Crown-6 Ether: A Molecular Dynamics Study. *J. Am. Chem. Soc.* **1995**, *117*, 6954−6960.
(32) Martinez, L.; Andrade, R.; Birgin, E. G.; Martinez, J. M. PACKMOL: A Package for Building Initial Configurations for Molecular Dynamics Simulations. *J. Comput. Chem.* **2009**, *30*, 2157−64.
(33) Yamashita, T.; Peng, Y.; Knight, C.; Voth, G. A. Computationally Efficient Multiconfigurational Reactive Molecular Dynamics. *J. Chem. Theory Comput.* **2012**, *8*, 4863−4875.
(34) Peng, Y.; Knight, C.; Blood, P.; Crosby, L.; Voth, G. A. Extending Parallel Scalability of Lammps and Multiscale Reactive Molecular Simulations. In *XSEDE '12: Proceedings of the 1st Conference of the Extreme Science and Engineering Discovery Environment: Bridging from the eXtreme to the campus and beyond, Proceedings of XSEDE12:2012 eXtreme Science and Engineering Discovery Environment, Chicago, Illinois, USA, July 16 - 20, 2012*; Association for Computing Machinery: New York, NY, United States, 2012; *37*, pp 1−7.
(35) Thompson, A. P.; Aktulga, H. M.; Berger, R.; Bolintineanu, D. S.; Brown, W. M.; Crozier, P. S.; in 't Veld, P. J.; Kohlmeyer, A.; Moore, S. G.; Nguyen, T. D.; et al. LAMMPS - a Flexible Simulation Tool for Particle-Based Materials Modeling at the Atomic, Meso, and Continuum Scales. *Comput. Phys. Commun.* **2022**, *271*, 108171.
(36) Tribello, G. A.; Bonomi, M.; Branduardi, D.; Camilloni, C.; Bussi, G. PLUMED 2: New Feathers for an Old Bird. *Comput. Phys. Commun.* **2014**, *185*, 604−613.
(37) Bonomi, M.; Bussi, G.; Camilloni, C.; Tribello, G. A.; Banáš, P.; Barducci, A.; Bernetti, M.; Bolhuis, P. G.; Bottaro, S.; Branduardi, D.; et al. Promoting Transparency and Reproducibility in Enhanced Molecular Simulations. *Nat. Methods* **2019**, *16*, 670−673.
(38) Kumar, S.; Rosenberg, J. M.; Bouzida, D.; Swendsen, R. H.; Kollman, P. A. The Weighted Histogram Analysis Method for Free-Energy Calculations on Biomolecules. I. The Method. *J. Comput. Chem.* **1992**, *13*, 1011−1021.
(39) Mazan, V.; Boltoeva, M. Y.; Tereshatov, E. E.; Folden, C. M. Mutual Solubility of Water and Hydrophobic Ionic Liquids in the Presence of Hydrochloric Acid. *RSC Adv.* **2016**, *6*, 56260−56270.
(40) Pace, C. N.; Laurents, D. V.; Erickson, R. E. Urea Denaturation of Barnase: pH Dependence and Characterization of the Unfolded State. *Biochemistry* **1992**, *31*, 2728−2734.
(41) Khalid, E. K.; Babiker, E. E.; El Tinay, A. H. Solubility and Functional Properties of Sesame Seed Proteins as Influenced by pH and/or Salt Concentration. *Food Chem.* **2003**, *82*, 361−366.
(42) Freire, M. G.; Carvalho, P. J.; Silva, A. M. S.; Santos, L. M. N. B. F.; Rebelo, L. P. N.; Marrucho, I. M.; Coutinho, J. A. P. Ion Specific Effects on the Mutual Solubilities of Water and Hydrophobic Ionic Liquids. *J. Phys. Chem. B* **2009**, *113*, 202−211.
(43) Hayduk, W. *Propane, Butane and 2-Methylpropane*; Pergamon Press: Oxford, UK, 1986; Vol. *24*.
(44) Carpenter, W. B.; Fournier, J. A.; Lewis, N. H. C.; Tokmakoff, A. Picosecond Proton Transfer Kinetics in Water Revealed with Ultrafast IR Spectroscopy. *J. Phys. Chem. B* **2018**, *122*, 2792−2802.
(45) Chiang, K.-Y.; Dalstein, L.; Wen, Y.-C. Affinity of Hydrated Protons at Intrinsic Water/Vapor Interface Revealed by Ion-Induced Water Alignment. *J. Phys. Chem. Lett.* **2020**, *11*, 696−701.
(46) Hillyer, M. B.; Gibb, B. C. Molecular Shape and the Hydrophobic Effect. *Annu. Rev. Phys. Chem.* **2016**, *67*, 307−329.
(47) Jiang, L.; Cao, S.; Cheung, P. P.-H.; Zheng, X.; Leung, C. W. T.; Peng, Q.; Shuai, Z.; Tang, B. Z.; Yao, S.; Huang, X. Real-Time Monitoring of Hydrophobic Aggregation Reveals a Critical Role of Cooperativity in Hydrophobic Effect. *Nat. Commun.* **2017**, *8*, 15639.
(48) Chandler, D. Interfaces and the Driving Force of Hydrophobic Assembly. *Nature* **2005**, *437*, 640−647.
(49) Ball, P. Water as an Active Constituent in Cell Biology. *Chem. Rev.* **2008**, *108*, 74−108.
(50) Nakashima, T.; Shimizu, M.; Kukizaki, M. Particle Control of Emulsion by Membrane Emulsification and Its Applications. *Adv. Drug Delivery Rev.* **2000**, *45*, 47−56.
(51) Ben-Amotz, D. Water-Mediated Hydrophobic Interactions. *Annu. Rev. Phys. Chem.* **2016**, *67*, 617−638.
(52) Huang, D. M.; Chandler, D. Temperature and Length Scale Dependence of Hydrophobic Effects and Their Possible Implications for Protein Folding. *Proc. Natl. Acad. Sci. U. S. A.* **2000**, *97*, 8324−8327.
(53) Shimizu, S.; Chan, H. S. Temperature Dependence of Hydrophobic Interactions: A Mean Force Perspective, Effects of Water Density, and Nonadditivity of Thermodynamic Signatures. *J. Chem. Phys.* **2000**, *113*, 4683−4700.
(54) Bogunia, M.; Makowski, M. Influence of Ionic Strength on Hydrophobic Interactions in Water: Dependence on Solute Size and Shape. *J. Phys. Chem. B* **2020**, *124*, 10326−10336.
(55) de Xammar Oro, J. R. Role of Co-Solute in Biomolecular Stability: Glucose, Urea and the Water Structure. *J. Biol. Phys.* **2001**, *27*, 73−79.
(56) Lo Nostro, P.; Ninham, B. W. Hofmeister Phenomena: An Update on Ion Specificity in Biology. *Chem. Rev.* **2012**, *112*, 2286−2322.
(57) Okur, H. I.; Hladílková, J.; Rembert, K. B.; Cho, Y.; Heyda, J.; Dzubiella, J.; Cremer, P. S.; Jungwirth, P. Beyond the Hofmeister Series: Ion-Specific Effects on Proteins and Their Biological Functions. *J. Phys. Chem. B* **2017**, *121*, 1997−2014.
(58) Morrison, T. J.; Billett, F. 730. The Salting-out of Non-Electrolytes. Part II. The Effect of Variation in Non-Electrolyte. *J. Chem. Soc.* **1952**, 3819−3822.
(59) Chen, X.; Yang, T.; Kataoka, S.; Cremer, P. S. Specific Ion Effects on Interfacial Water Structure near Macromolecules. *J. Am. Chem. Soc.* **2007**, *129*, 12272−12279.
(60) Du, Q.; Freysz, E.; Shen, Y. R. Surface Vibrational Spectroscopic Studies of Hydrogen Bonding and Hydrophobicity. *Science* **1994**, *264*, 826−828.

https://doi.org/10.1021/acs.jpcb.3c00828
J. Phys. Chem. B 2023, 127, 3911−3918